Constraints on the anomalous $Z\gamma\gamma$ and $ZZ\gamma$ vertices at Next Linear Collider energies

R. Walsh* and A. J. Ramalho†
Instituto de Física, Universidade Federal do Rio de Janeiro, Caixa Postal 68528, Ilha do Fundão, 21945-970 Rio de Janeiro, RJ, Brazil

(Received 18 August 1997; revised manuscript received 16 December 1997; published 23 March 1998)

We study the effect of anomalous CP-conserving gauge boson couplings of the $Z\gamma\gamma$ and $ZZ\gamma$ vertices on the reaction $e^+e^-\to\gamma Z^*\to\gamma\mu^+\mu^-$ at NLC energies. Limits on these trilinear couplings are obtained at the 95% confidence level for different form factor scales, assuming that any other neutral gauge boson couplings vanish at the tree level. [S0556-2821(98)00309-9]

PACS number(s): 12.60.Cn, 12.15.Ji

I. INTRODUCTION

An important goal of the next generation of linear e^+e^- colliders [Next Linear Collider (NLC)] is to search for possible deviations from the standard model of electroweak interactions. Several collaborations are currently studying the physics potential and developing feasible designs for these machines at test facilities. In particular, these colliders will be very useful to investigate both the form and strength of the self-interactions of the electroweak gauge bosons, which are determined in the standard model by an underlying $SU(2)\times U(1)$ gauge symmetry. Any deviation of these couplings from their standard model values would point to new physics. Anomalous gauge boson couplings have been extensively discussed in the literature [1]. Although the structures of the $WW\gamma$ and WWZ vertices have received the most attention, some theorists have emphasized the importance of measuring neutral boson self-couplings [2,3], and over the last years, considerable effort has been made by experimentalists to search for anomalous $Z\gamma\gamma$ and $ZZ\gamma$ couplings [4,5].

In this paper we analyze the CP-conserving structure of the $Z\gamma\gamma$ and $ZZ\gamma$ vertices through the differential cross sections for the process $e^-e^+\to\gamma Z^*\to\gamma\mu^+\mu^-$ at NLC c.m. energy $\sqrt{s}=500$ GeV and an integrated luminosity of 10 fb^{-1}. The most general Lorentz and gauge invariant, CP-conserving $ZZ\gamma$ vertex in momentum space is given by [3]

$$V^{\alpha\beta\mu}_{Z\gamma Z}(k,p,q)=ie\frac{q^2-k^2}{M_Z^2}\left(h_3^Z\varepsilon^{\mu\alpha\beta\rho}p_\rho+\frac{h_4^Z}{M_Z^2}\varepsilon^{\mu\beta\rho\sigma}q^\alpha q_\rho p_\sigma\right).$$

The index assignments and momentum flow are represented in Fig. 1. The corresponding $Z\gamma\gamma$ vertex can be obtained from the expression above by the substitutions $q^2-k^2\to q^2$ and $h^Z_{3,4}\to h^\gamma_{3,4}$. The anomalous couplings h_3^V and h_4^V, where $V=\gamma,Z$, are form factors which vanish at asymptotically high energies. Following Ref. [3], we take these energy-dependent anomalous couplings to have the dipole form

$$h_i^V(q^2)=\frac{h_{i0}^V}{(1+q^2/\Lambda^2)^{n_i}},\quad i=3,4,\quad V=\gamma,Z,$$

where $n_3=3$ and $n_4=4$. Λ is some large energy scale around which the new nonstandard physics would set in. The bounds on the anomalous $Z\gamma\gamma$ and $ZZ\gamma$ couplings established by the D0 Collaboration at the Fermilab Tevatron $p\bar{p}$ Collider are the most stringent experimental limits currently available [5]. For a form factor scale $\Lambda=750$ GeV and combining the decay modes $Z\to\mu\mu,ee,\nu\nu$, the 95% C.L. limits are $|h^\gamma_{30}|<0.45$, $|h^\gamma_{40}|<0.06$, $|h^Z_{30}|<0.44$, and $|h^Z_{40}|<0.06$.

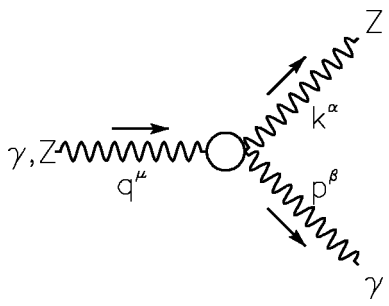

FIG. 1. Neutral boson trilinear vertices.

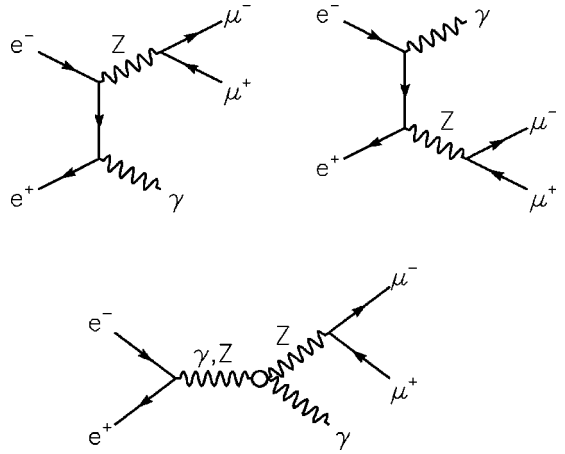

FIG. 2. Feynman diagrams of the process $e^-e^+\to\gamma$, $Z^*\to\gamma\mu^+\mu^-$.

*Email address: walsh@if.ufrj.br
†Email address: ramalho@if.ufrj.br

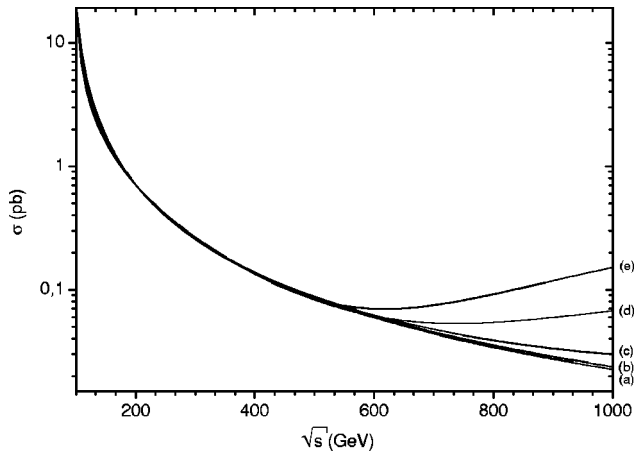

FIG. 3. Dependence of the total cross section on the c.m. energy $\sqrt{s}$, for an input scale $\Lambda=1.5$ TeV. Curve (a) represents the standard model prediction, while curves (b) and (c) correspond to the anomalous couplings $(h_{30}^V,h_{40}^V)=(10^{-2},0)$ with $V=Z$ and $V=\gamma$, respectively. Curves (d) and (e) correspond to $(h_{30}^V,h_{40}^V)=(0,10^{-3})$ with $V=Z$ and $V=\gamma$, respectively.

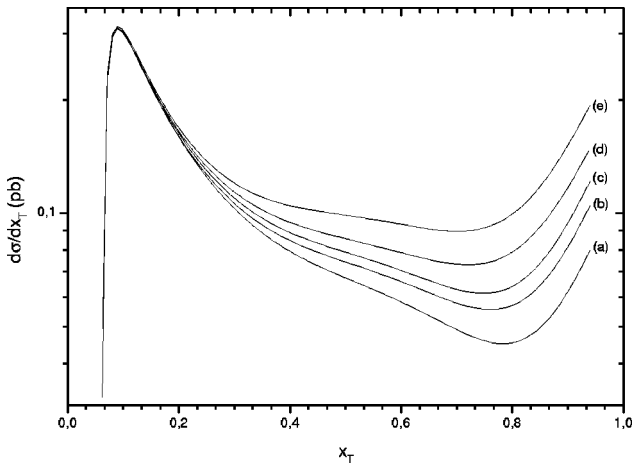

FIG. 4. Transverse momentum distribution for the photon, for an input scale $\Lambda=1.5$ TeV. (a) represents the standard model prediction, while (b) and (d) correspond to the anomalous couplings $(h_{30}^V,h_{40}^V)=(3\times10^{-2},0)$ with $V=Z$ and $V=\gamma$, respectively. Curves (c) and (e) correspond to $(h_{30}^V,h_{40}^V)=(0,3\times10^{-3})$ with $V=Z$ and $V=\gamma$, respectively.

II. CROSS SECTIONS AND LIMITS

In order to find distributions most sensitive to anomalous $Z\gamma\gamma$ and $ZZ\gamma$ couplings, we carried out a Monte Carlo simulation of the process $e^-e^+\to\gamma Z^*\to\gamma\mu^+\mu^-$. The relevant Feynman diagrams are shown in Fig. 2. The corresponding amplitudes were written in a form suitable for numerical evaluation. For the electroweak parameters we used $\sin^2\theta_W=0.23$, $M_Z=91.187$ GeV, $\Gamma_Z=2.49$ GeV, and $\alpha(M_Z^2)=1/128$. To take into account typical detector acceptances, we imposed a 5 GeV cut on the energy of the final-state photon, and required that the photon emerge with a polar angle θ_γ, measured with respect to the direction of the incoming electron beam, in the range $5°<\theta_\gamma<175°$. Figure 3 shows the total cross section of the process under discussion, as a function of the center-of-mass energy. At $\sqrt{s}=500$ GeV the total event rates for models with anomalous couplings are comparable to the rate in the standard model, corresponding to a total number of events of the order of 10^3 for a conservative integrated luminosity of 10 fb^{-1}. Several kinematical distributions were calculated and the transverse momentum distribution of the photon was found to be the most sensitive to the anomalous couplings. In general, the distributions are more sensitive to h_4^V than to h_3^V. Figure 4 shows the transverse momentum distribution $d\sigma/dx_T$ in terms of the scaled variable $x_T\equiv 2k_T/\sqrt{s}$, where k_T is the photon transverse momentum, both for the standard model and for anomalous couplings. All nonstandard distributions were calculated with $\Lambda=1.5$ TeV. The curves show a peak around $x_T\sim0.1$, which corresponds to contributions from those events in which an energetic photon comes out with small angles. The position of this peak is determined basically by the angular cut. The deviations from the standard model increase for moderate and large values of the photon transverse momentum, the more so in the presence of nonzero form factors h_4^V. In fact, at the energy $\sqrt{s}=500$ GeV the sensitivity of $d\sigma/dx_T$ to h_3^V and h_4^V depends essentially on the region $x_T\gtrsim0.8$, and is not reduced by a more stringent cut at the lower end of the x_T spectrum.

From the photon transverse-momentum spectra the confidence intervals for the form factors were determined by a χ^2 analysis. The x_T interval was divided into $n_B=6$ bins and the χ^2 function defined as

$$\chi^2=\sum_{i=1}^{n_B}\left(\frac{N_i^{SM}-N_i^{AN}}{\Delta N_i^{SM}}\right)^2,$$

where N_i^{SM} and N_i^{AN} stand for the number of events in the ith bin predicted by the standard model and in the presence of anomalous couplings, respectively, and $\Delta N_i^{SM}=\sqrt{N_i^{SM}+(N_i^{SM}\delta)^2}$ represents the corresponding statistical and systematic errors added in quadrature. We considered a systematic error $\delta=2\%$ for a measurement.

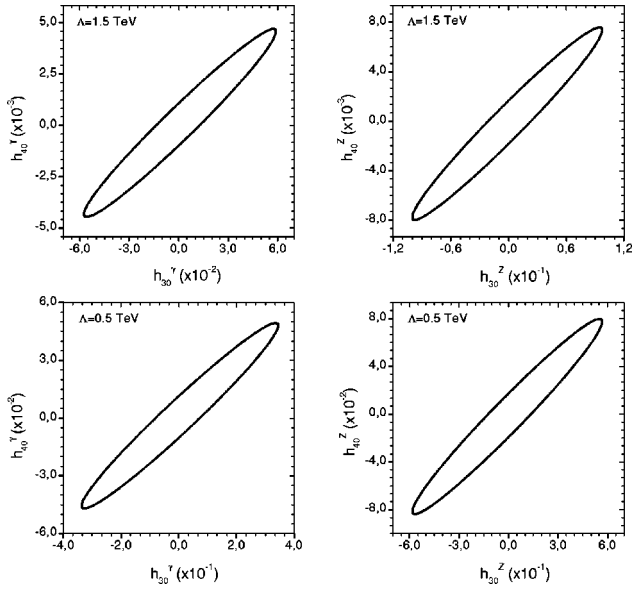

FIG. 5. 95% C.L. contours in the $h_{30}^\gamma-h_{40}^\gamma$ and $h_{30}^Z-h_{40}^Z$ planes both for $\Lambda=1.5$ TeV and $\Lambda=0.5$ TeV.

TABLE I. 95% C.L. bounds on the form factors for $\Lambda=0.5$ TeV and $\Lambda=1.5$ TeV. (a) Concerns the correlated limits derived from Fig. 5, (b) the correlated limits in the presence of both the $Z\gamma\gamma$ and $ZZ\gamma$ (Figs. 6 and 7), and (c) the one-degree-of-freedom constraints on the form factors.

Coupling	$\Lambda=1.5$ TeV		$\Lambda=0.5$ TeV	
		(a)		
h_{30}^{γ}	-5.83×10^{-2}	$+5.95\times10^{-2}$	-3.41×10^{-1}	$+3.49\times10^{-1}$
h_{40}^{γ}	-4.53×10^{-3}	$+4.77\times10^{-3}$	-4.78×10^{-2}	$+5.03\times10^{-2}$
h_{30}^{Z}	-1.01×10^{-1}	$+9.86\times10^{-2}$	-5.91×10^{-1}	$+5.75\times10^{-1}$
h_{40}^{Z}	-8.11×10^{-3}	$+7.73\times10^{-3}$	-8.51×10^{-2}	$+8.12\times10^{-2}$
		(b)		
h_{30}^{γ}	-1.40×10^{-2}	$+1.40\times10^{-2}$	-8.24×10^{-2}	$+8.17\times10^{-2}$
h_{40}^{γ}	-1.10×10^{-3}	$+1.11\times10^{-3}$	-1.15×10^{-2}	$+1.16\times10^{-2}$
h_{30}^{Z}	-2.24×10^{-2}	$+2.46\times10^{-2}$	-1.31×10^{-1}	$+1.44\times10^{-1}$
h_{40}^{Z}	-1.95×10^{-3}	$+1.76\times10^{-3}$	-2.03×10^{-2}	$+1.84\times10^{-2}$
		(c)		
h_{30}^{γ}	-1.21×10^{-2}	$+1.12\times10^{-2}$	-7.07×10^{-2}	$+6.53\times10^{-2}$
h_{40}^{γ}	-8.75×10^{-4}	$+9.51\times10^{-4}$	-1.11×10^{-2}	$+1.00\times10^{-2}$
h_{30}^{Z}	-1.89×10^{-2}	$+2.10\times10^{-2}$	-1.10×10^{-1}	$+1.23\times10^{-1}$
h_{40}^{Z}	-1.65×10^{-3}	$+1.48\times10^{-3}$	-1.73×10^{-2}	$+1.55\times10^{-2}$

First, we obtained the $h_{30}^{V}-h_{40}^{V}$ confidence regions for the case where anomalous couplings arise either from the $Z\gamma\gamma$ or from the $ZZ\gamma$ vertex. Figure 5 shows the 95% C.L. ellipses in the $h_{30}^{\gamma}-h_{40}^{\gamma}$ and $h_{30}^{Z}-h_{40}^{Z}$ planes, both for $\Lambda=0.5$ TeV and $\Lambda=1.5$ TeV. Clearly, the sensitivity of the transverse momentum distribution to variation in h_{30}^{V} and h_{40}^{V} increases with Λ. The correlated bounds derived from Fig. 5 are displayed in section (a) of Table I. We also computed kinematic distributions using longitudinally polarized electron beams and determined the 95% C.L. exclusion contours thereof. Considering the occurrence of only one anomalous vertex (either $Z\gamma\gamma$ or $ZZ\gamma$), the gains in sensitivity were negligible and the 95% C.L. ellipses were found to be essentially the same as those in Fig. 5.

Next we analyzed the pairwise correlated limits for couplings arising from the $Z\gamma\gamma$ and $ZZ\gamma$ vertices. In Figs. 6 and 7 the central ellipses result from the photon x_T distribution with unpolarized electron beams, whereas the larger ellipses were obtained from polarized x_T distributions. Here one sees that longitudinally polarized electron beams can be useful to constrain even further the allowed regions in the parameter spaces. The simultaneous presence of $Z\gamma\gamma$ and $ZZ\gamma$ vertices gives rise to important interference terms whose contribu-

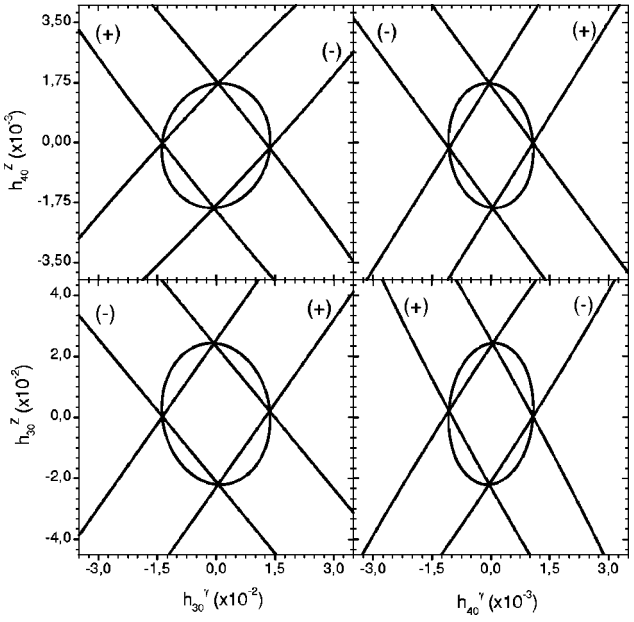

FIG. 6. 95% C.L. contours for pairs of form factors, one of which comes from the $Z\gamma\gamma$ vertex while the other comes from the $ZZ\gamma$ for a scale $\Lambda=1.5$ TeV. The $(\pm)$ signs beside the long ellipses refer to the helicity of the incoming electrons.

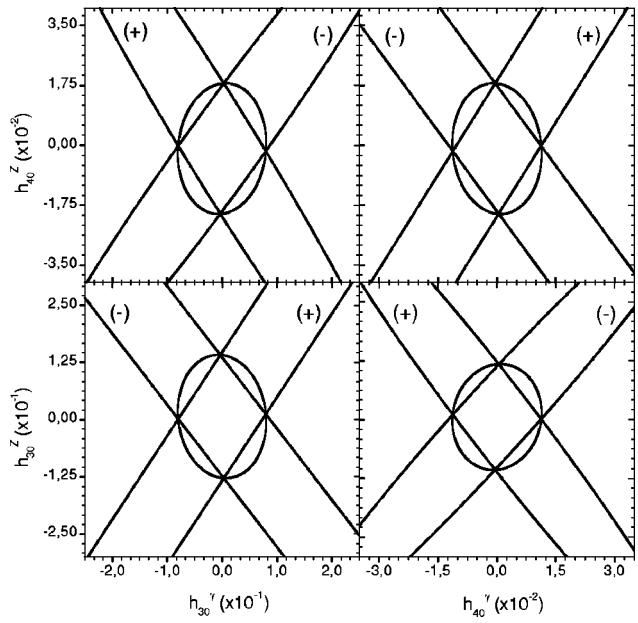

FIG. 7. Same as Fig. 6 but for a form factor scale $\Lambda=0.5$ TeV.

tions roughly cancel out in the unpolarized cross sections. For definite-helicity electron beams, however, some of these interference contributions survive, leading to the oblique ellipses in Figs. 6 and 7. The correlated bounds that result from Figs. 6 and 7 are shown in section (b) of Table I. We also varied each form factor, while keeping all the others at their standard model values. These individual 95% C.L. constraints are presented in section (c) of Table I. They are at least one order of magnitude more restrictive than the present experimental bounds.

ACKNOWLEDGMENTS

This work was partly supported by CNPq and FINEP.

[1] T. Barklow *et al.*, Report No. SLAC-PUB-7366, and references therein.

[2] F. M. Renard, Nucl. Phys. **B196**, 93 (1982); P. Méry, M. Perrottet, and F. M. Renard, Z. Phys. C **38**, 579 (1988); L. Bento and A. Barroso, Phys. Rev. D **38**, 2742 (1988); F. Boudjema, in e^+e^- *Collisions at 500 GeV: The Physics Potential*, Proceedings of the Workshop Munich, Annecy, Hamburg, 1991, edited by P. M. Zerwas (DESY Report No. 92-123B, Hamburg, 1992), p. 757; D. Choudhury and S. D. Rindani, Phys. Lett. B **335**, 198 (1994); D. Chang, W. Keung, and P. Pal, Phys. Rev. D **51**, 1326 (1995); T. G. Rizzo, *ibid.* **54**, 3057 (1996).

[3] U. Baur and E. L. Berger, Phys. Rev. D **47**, 4889 (1993).

[4] L3 Collaboration, M. Acciarri *et al.*, Phys. Lett. B **346**, 190 (1995); CDF Collaboration, F. Abe *et al.*, Phys. Rev. Lett. **74**, 1941 (1995); D0 Collaboration, S. Abachi *et al.*, *ibid.* **75**, 1028 (1995); DELPHI Collaboration, W. Adam *et al.*, Phys. Lett. B **380**, 471 (1996).

[5] D0 Collaboration, S. Abachi *et al.*, Phys. Rev. Lett. **78**, 3640 (1997).